# Atomic-Scale Structure of Nanocrystalline $Ba_xSr_{1-x}TiO_3$ ($x = 1, 0.5, 0$) by X-ray Diffraction and the Atomic Pair Distribution Function Technique

Valeri Petkov,*[,†] Milen Gateshki,[†] Markus Niederberger,[‡] and Yang Ren[§]

*Department of Physics, Central Michigan University, Mt. Pleasant, Michigan 48859, Max-Planck Institute of Colloids and Interfaces, Potsdam D-14424, Germany, and Advanced Photon Source, Argonne National Laboratory, Argonne, Illinois 60439*

*Received September 23, 2005. Revised Manuscript Received November 13, 2005*

The atomic-scale structure of nanocrystalline $Ba_xSr_{1-x}TiO_3$ ($x = 1, 0.5, 0$) powders has been studied using high-energy X-ray diffraction, Rietveld refinement, and the atomic pair distribution function technique. The studies show that the materials are well-ordered at nanometer length distances. The three-dimensional atomic ordering in $Ba_{0.5}Sr_{0.5}TiO_3$ and $SrTiO_3$ nanopowders may well be described by a cubic structure of the perovskite type, similar to that occurring in the corresponding bulk crystals. The three-dimensional atomic ordering in $BaTiO_3$ is more complex. It is cubic-like on average, but locally shows slight distortions of a tetragonal-type. The new structural information helps one to understand better the dielectric properties of these nanomaterials.

## 1. Introduction

Crystalline perovskite-type oxides show many useful properties and are widely used as catalysts and in piezoelectrics and ferroelectrics.[1,2] A prime example is the family of $Ba_xSr_{1-x}TiO_3$ oxides, in particular, $BaTiO_3$. The material exists in several crystallographic modifications, each showing a particular dielectric behavior. At high temperature $BaTiO_3$ has a centrosymmetric cubic structure and is paraelectric. Between room temperature and 393 K the material possesses a tetragonal-type structure, below 278 K the structure is orthorhombic, and below 183 K it is rhombohedral.[3] Fragments of the four polymorphs occurring with $BaTiO_3$ are presented in Figure 1. The picture is characteristic of perovskites: all crystalline modifications of $(Ba/Sr)TiO_3$ feature a three-dimensional network of $Ti-O_6$ octahedra with Ba/Sr atoms occupying the network channels. The asymmetry of the low-temperature crystallographic modifications arises from a displacement of the Ti cations with respect to the oxygen octahedra (as depicted in Figures 1b−1d) and gives rise to spontaneous polarization. As a result, $BaTiO_3$ becomes ferroelectric below 393 K. The high permittivity of the tetragonal modification of $BaTiO_3$ and the ability to switch the direction of polarization in response to external electric fields have found application in commercially available devices such as thin film and multilayer capacitors.[4,5]

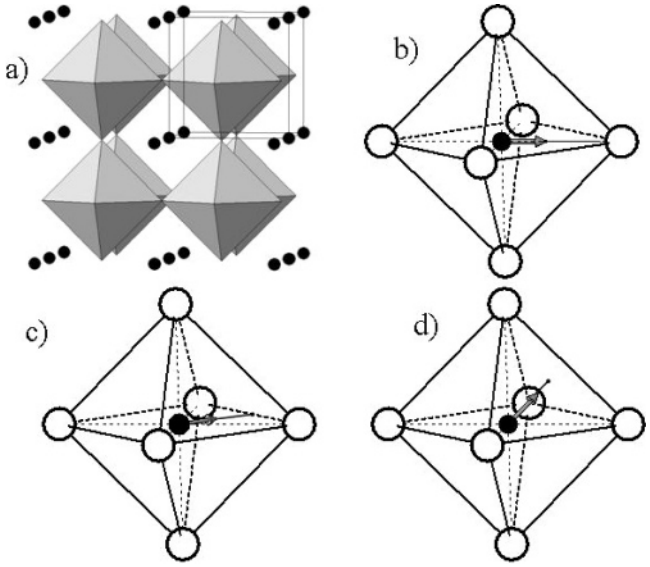


**Figure 1.** Fragments of the cubic- (a), tetragonal- (b), orthorhombic- (c), and rhombohedral-type (d) structures occurring with bulk $BaTiO_3$ crystals. All structure types feature a 3D network of corner-sharing $Ti-O_6$ octahedra with Ba atoms (solid circles) occupying the open space between them as shown in (a). Note the octahedral units are perfect in the cubic-type structure. The $Ti-O_6$ octahedra shown are somewhat distorted with the non-cubic-type structure types due to the off-center displacement (directions shown with arrows) of Ti atoms (solid circles at the center of the octahedra) as depicted in (b), (c), and (d). The octahedra are centered by Ti atoms (small solid circles) and coordinated by oxygens (open cicles). The unit cell in the case of the cubic-type perovskite structure is outlined with thin solid lines.

$SrTiO_3$ is a typical perovskite possessing a cubic structure (see Figure 1a) at room temperature. Although $BaTiO_3$ and $SrTiO_3$ have structures of a similar (perovskite) type, they show very different transition behavior. It is not until $SrTiO_3$ is cooled to 110 K when its cubic structure distorts and

* To whom correspondence should be addressed. E-mail: petkov@phy.cmich.edu.
† Central Michigan University.
‡ Max-Planck Institute of Colloids and Interfaces.
§ Argonne National Laboratory.

(1) Chandler, C. D.; Roger C.; Hampden-Smith, M. J. *Chem. Rev.* **1993**, *93*, 1205.
(2) Bhalla, A. S.; Gou, R.; Roy, R. *Mater. Res. Innovations* **2000**, *4*, 3.
(3) Kwei, G.; Billinge, S. J. L.; Cheong, S.-W.; Saxton, J. G. *Ferroelectrics* **1995**, *164*, 57.
(4) Hennings, D.; Klee, M.; Waser, R. *Adv. Mater.* **1991**, *3*, 334.
(5) Frey, M. H.; Payne, D. A. *Appl. Phys. Lett.* **1993**, *63*, 2753.

10.1021/cm052145g CCC: $33.50 
Published on Web 01/13/2006

becomes tetragonal.[6,7] Thus, $SrTiO_3$ exhibits paraelectric behavior at room temperature, although recent studies suggest that the material is indeed an incipient ferroelectric whose ferroelectricity is suppressed by quantum fluctuations.[8]

Barium-based mixed oxides have also attracted much attention.[9] In particular, $Ba_xSr_{1-x}TiO_3$ has shown excellent dielectric properties, especially as thin films. At room temperature and low concentrations of Sr ($x < 0.5$) these mixed oxides adopt a tetragonal-type structure[10] featuring slightly distorted $Ti-O_6$ octahedra (see Figure 1b). At higher concentrations of Sr the structure is of the cubic type shown in Figure 1a.[11]

It has been discovered that many of the useful properties of perovskite materials are critically dependent on the crystallite size. For example, it has been found that at room temperature the structure of $BaTiO_3$ transforms to cubic-like when the crystallite size becomes smaller than 100 nm.[12,13] On the other hand, high-resolution synchrotron radiation studies and Raman scattering experiments have shown that fine $BaTiO_3$ powders with crystallite size as small as 40 nm show a structure with tetragonal distortions and exhibit somewhat reduced but still measurable spontaneous polarization.[14] Recently, the attention has shifted to even finer powders with crystallites as small as only a few nanometers. The reason is that having $Ba_xSr_{1-x}TiO_3$ in a nanocrystalline state is a key requirement for producing defect-free thin films.[15,16] Furthermore, nanosize powders provide good sinterability, which is an essential property for the fabrication of advanced ceramic materials.[2,4]

When in a nanocrystalline state $Ba_xSr_{1-x}TiO_3$ ceramics are non-ferroelectric, resulting in stable dielectric properties.[17,18] Several explanations for the disappearance of ferroelectricity have been put forward. They point to the absence of long-range cooperative structural distortions as one of the main reasons that could lead to a suppression of the thermodynamically stable tetragonal phase and the related to it ferroelectric behavior in nanostructured $Ba_xSr_{1-x}TiO_3$.[19] A thorough understanding of this so-called size effect and the properties of nanocrystalline barium/strontium-based materials obviously requires a detailed knowledge of their atomic-scale structure. Usually the structure of materials is determined from the Bragg peaks in their diffraction patterns. However, nanocrystalline materials lack the extended order of the usual crystals and show diffraction patterns with a pronounced diffuse component and a few broad Bragg-like features. This renders the traditional diffraction techniques for structure determination very difficult to apply. That is why structural studies on nanocrystals are scarce and the atomic arrangement in $Ba_xSr_{1-x}TiO_3$ nanopowders has not been determined in detail yet. Recently, it has been shown that the three-dimensional (3D) structure of materials with reduced structural coherence, including nanocrystals, can be determined using the so-called atomic pair distribution function (PDF) technique.[20−23] Here, we employ the traditional Rietveld and the nontraditional PDF technique to determine the 3D structure of $Ba_xSr_{1-x}TiO_3$ ($x = 1$, 0.5, 0) nanoparticles with crystallites having size as small as 5 nm. We find that these nanostructured materials possess a well-defined atomic arrangement that may be described in terms of the perovskite-type structure depicted in Figure 1. The new structural information helps one understand better the dielectric properties of the nanomaterials.

## 2. Experimental Section

**2.1. Sample Preparation.** Nanocrystalline $Ba_xSr_{1-x}TiO_3$ samples were obtained through a recently discovered approach employing a nonhydrolytic and halide-free procedure.[24] In the first step of the procedure metallic barium and/or strontium were dissolved in anhydrous benzyl alcohol at elevated temperatures (343−373 K). Generally, Sr needed a higher temperature to dissolve than Ba. The resulted solutions were mixed with 1 molar equiv of titanium isopropoxide, and the reaction mixture was transferred to a steel autoclave and heated at 574 K for 48 h. The heating took place under subsolvothermal conditions since the boiling point of benzyl alcohol is about 478 K. Representative TEM images of thus-obtained nanocrystalline materials are shown in Figures 2, 3, and 4 in ref 24. The TEM images reveal that the samples consist of individual particles with an average size of about 5 nm. Analyses based on the width of the peaks in the X-ray diffraction patterns of $Ba_xSr_{1-x}TiO_3$ performed by us yielded very similar estimates for the average nanocrystallites' size. The TEM studies also show that the nanocrystals are uniform in size and mostly spherical. No large particles or agglomerates are observed. Thus-obtained nanocrystalline $Ba_xSr_{1-x}TiO_3$ ($x = 1$, 0.5, 0) powders were loaded into glass capillaries and subjected to synchrotron radiation scattering experiments.

**2.2. Synchrotron Radiation Scattering Experiments.** Synchrotron radiation scattering experiments were carried out at the beamline 11-ID-C (Advanced Photon Source, Argonne National Laboratory) using X-rays of energy 115.232 keV ($\lambda = 0.1076$ Å) at room temperature. X-rays of higher energy were used to obtain diffraction data to higher values of the wave vector, $Q$, which is important for the success of PDF analysis ($Q_{max} = 28$ Å$^{-1}$ with

(6) Lytle, F. W. *J. Appl. Phys.* **1964**, *35*, 2212.
(7) Salje, E. K.; Gallardo, M. C.; Jimenes, J.; Cerro, J. *J. Phys.: Condens. Matter* **1998**, *10*, 5535.
(8) Wang, Y. X. *Solid State Commun.* **2005**, *135*, 290.
(9) Thongrueng, J.; Nishio, K.; Watanable, Y.; Nagata, K.; Tsuchiya, T. *J. Aust. Ceram. Soc.* **2001**, *37*, 51.
(10) Josef, J.; Vimala, T. M.; Raju, J.; Murthy, V. R. K. *J. Appl. Phys.* **1999**, *32*, 1049.
(11) Liu, R. S.; Cheng, Y. C.; Chen, J. M.; Liu, R. G.; Wang, J. L.; Tsai, J. C.; Hsu, M. Y. *Mater. Lett.* **1998**, *37*, 285.
(12) Uchino, K.; Sadanaga, E.; Hirose, T. *J. Am. Ceram. Soc.* **1989**, *72*, 1151.
(13) Begg, B. D.; Vance, E. R.; Nowotny, J. *J. Am. Ceram. Soc.* **1994**, *77*, 3186.
(14) Yashimura, M.; Hoshina, T.; Ishimura, D.; Kobayashi, S.; Nakamura, W.; Tsurumi, T.; Wada, S. *J. Appl. Phys.* **2005**, *98*, 014313.
(15) Matsuda, H.; Kobayashi, N.; Kobayashi, T.; Miyazawa, K.; Kuwabara, N. *J. Non-Cryst. Solids* **2000**, *271*, 162.
(16) Zhang, J.; Yin, Z.; Zhang, M.-S. *Phys. Lett. A* **2003**, *310*, 479.
(17) Takeuchi, T.; Tabuchi, M.; Ado, K.; Honjo, K.; Nakamura, O.; Kageyama, H.; Suyama, Y.; Ohtori, N.; Nagasawa, M. *J. Mater. Sci.* **1997**, *32*, 4053.
(18) Soten, I.; Miguez, H.; Yang, S. M.; Petrov, S.; Coombs, N.; Tetreault, N.; Matsuura, N.; Ruda, H. E.; Ozin, G. *Adv. Funct. Mater.* **2002**, 12.
(19) Frey, M. H.; Payne, D. A. *Phys. Rev. B* **1996**, *54*, 3158.
(20) Toby, B. H.; Egami T. *Acta Crystallogr. A* **1992**, *48*, 336.
(21) Gateshki, M.; Hwang, S.-J.; Park, D. H.; Ren, Y.; Petkov, V. *J. Phys. Chem. B* **2004**, *108*, 14956.
(22) Billinge, S. J. L.; Kanatzidis, M. G. *Chem. Commun.* **2004**, *7*, 749.
(23) Petkov, V.; Trikalitis, P. N.; Bozin, E. S.; Billinge, S. J. L.; Vogt, T.; Kanatzidis, M. G. *J. Am. Chem. Soc.* **2002**, *124*, 10157.
(24) (a) Niederberger, M.; Pinna, N.; Polleux, J.; Antonietti, M. *Angew. Chem., Int. Ed.* **2004**, *43*, 2270. (b) Niederberger, M.; Garnweitner, G.; Pinna, N.; Antoneitti, M. *J. Am. Chem. Soc.* **2004**, *126*, 9120.

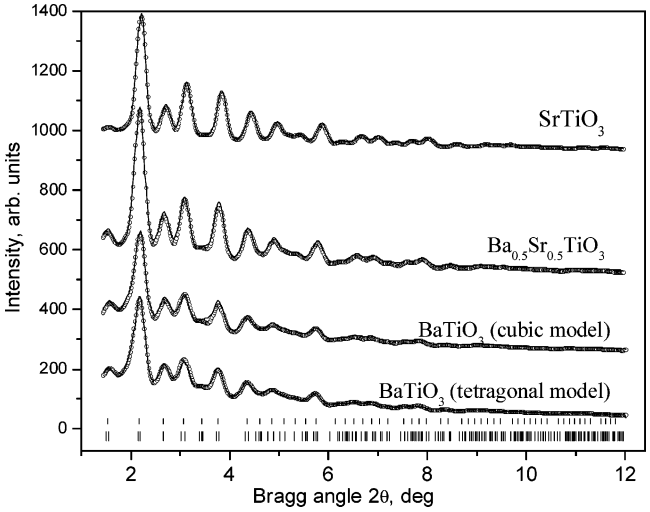


**Figure 2.** Experimental powder diffraction patterns for nanocrystalline $Ba_xSr_{1-x}TiO_3$ (symbols) and calculated patterns (solid lines) obtained through Rietveld refinements. The positions of the Bragg peaks of the cubic (upper set of bars) and tetragonal (lower set of bars) structures that were fitted to the diffraction pattern of $BaTiO_3$ are given in the lower part of the plot. Note the diffraction data for $SrTiO_3$ and $Ba_{0.5}Sr_{0.5}TiO_3$ are approximated with a cubic-type structure only. The corresponding goodness-of-fit factors, $R_w$, for each of the refinements are reported in Table 1.

the present experiments). The scattered radiation was collected with an imaging plate detector (mar345). The use of an imaging plate detector greatly reduces the data collection time and improves the statistical accuracy of the diffraction data as demonstrated by recent experiments on materials with reduced structural coherence.[25] Up to 10 images were taken for each of the samples. The exposure time was 10 s/image. The corresponding images were combined, subjected to geometrical corrections, integrated, and reduced to one-dimensional X-ray diffraction (XRD) patterns using the computer program FIT2D.[26] Thus-obtained XRD patterns for the three samples studied are presented in Figure 2.

## 3. Results

As can be seen in Figure 2, the experimental XRD patterns of nanocrystalline $Ba_xSr_{1-x}TiO_3$ powders show only a few broad, Bragg-like peaks that merge into a slowly oscillating diffuse component already at Bragg angles as low as 6°. As our subsequent analyses show, the diffraction patterns of $SrTiO_3$ and $Ba_{0.5}Sr_{0.5}TiO_3$ can be indexed in a cubic unit cell while that of $BaTiO_3$ can be indexed in both cubic and tetragonal unit cells of the perovsike-type structure type shown in Figure 1. Such diffraction patterns are typical for materials of limited structural coherence and are obviously difficult to be tackled by traditional techniques for structure determination. However, when reduced to the corresponding atomic PDFs, they become a structure-sensitive quantity lending itself to structure determination.

The frequently used atomic Pair Distribution Function, $G(r)$, is defined as

$$G(r) = 4\pi r[\rho(r) - \rho_0] \qquad (1)$$

where $\rho(r)$ and $\rho_0$ are the local and average atomic number densities, respectively, and $r$ is the radial distance. It peaks at characteristic distances separating pairs of atoms and thus reflects the atomic-scale structure. The PDF $G(r)$ is the Fourier transform of the experimentally observable total structure function, $S(Q)$, i.e.,

$$G(r) = (2/\pi)\int_{Q=0}^{Q_{max}} Q[S(Q) - 1]\sin(Qr)\, dQ \qquad (2)$$

where $Q$ is the magnitude of the wave vector ($Q = 4\pi \sin\theta/\lambda$), $2\theta$ is the angle between the incoming and outgoing radiation beams, and $\lambda$ is the wavelength of the radiation used. The structure function is related to the coherent part of the total scattered intensity as

$$S(Q) = 1 + [I^{coh}(Q) - \sum c_i|f_i(Q)|^2]/|\sum c_i f_i(Q)|^2 \qquad (3)$$

where $I^{coh}(Q)$ is the coherent scattering intensity per atom in electron units and $c_i$ and $f_i$ are the atomic concentration and X-ray scattering factor, respectively, for the atomic species of type $i$.[27] As can be seen from eqs 1−3, the PDF is simply another representation of the powder XRD data. However, exploring the diffraction data in real space is advantageous, especially in the case of materials of limited structural coherence. First, as eqs 2 and 3 imply, the *total* scattering, including Bragg scattering as well as diffuse scattering, contributes to the PDF. In this way both the average, longer range atomic structure, manifested in the Bragg peaks, and the local structural distortions, manifested in the diffuse component of the diffraction pattern, are reflected in the PDF. And second, the atomic PDFs do not imply any periodicity and can be used to study the atomic ordering in materials showing any degree of structural coherence, ranging from crystals[28] to glasses[29] and even liquids.[30] Recently, the atomic PDF approach has been successfully applied to nanocrystalline materials[31−33] as well.

Experimental PDFs for the samples studied were obtained as follows. First, the coherently scattered intensities were extracted from the corresponding XRD patterns by applying appropriate corrections for flux, background, Compton scattering, and sample absorption. The intensities were normalized in absolute electron units, reduced to structure functions $Q[S(Q) - 1]$, and Fourier-transformed to atomic PDFs. Thus-obtained experimental atomic PDFs are shown in Figure 3. All data processing was done with the help of the program RAD.[34] As can be seen in Figure 3, the experimental PDFs are rich in structural features but they vanish at interatomic distances of 2−2.5 nm which are much shorter than the average size of the nanocrystals (∼5 nm).

(25) (a) Chupas, P. J.; Qiu, X.; Lee, P.; Grey C. P.; Billinge, S. J. L. *J. Appl. Crystallogr.* **2003**, *36*, 1342. (b) Petkov, V.; Qadir, D.; Shastri, S. D. *Solid State Commun.* **2004**, *129*, 239.
(26) Hammersley, A. P.; Hanfland, M.; Hausermann, D. *High-Pressure Res.* **1996**, *14*, 235.
(27) Klug, H. P.; Alexander, L. E. In *X-ray Diffraction Procedures for Polycrystalline Materials*; Wiley: New York, 1974.
(28) Petkov, V.; Jeong, I.-K.; Chung, J. S.; Thorpe, M. F.; Kycia, S.; Billinge, S. J. L. *Phys. Rev. Lett.* **1999**, *83*, 4089.
(29) Petkov, V.; Billinge, S. J. L.; Sashtri, S. D.; Himmel, B. *Phys. Rev. Lett.* **2000**, *85*, 3436.
(30) Petkov, V.; Yunchov, G. *J. Phys.: Condens. Matter* **1996**, *8*, 6145.
(31) Petkov, V.; Zavalij, P. Y.; Lutta, S.; Whittingham, M. S.; Parvanov, V.; Shastri, S. D. *Phys. Rev. B* **2004**, *69*, 085410.
(32) Dmowski, W.; Egami, T.; Swider-Lyons, K. E.; Love, C. T.; Rolison, D. R. *J. Phys. Chem. B* **2002**, *106*, 12677.
(33) Gateshki, M.; Petkov, V.; Williams, G.; Pradhan S. K.; Ren, Y. *Phys. Rev. B* **2005**, *71*, 224107.
(34) Petkov, V. *J. Appl. Crystallogr.* **1989**, *22*, 387.

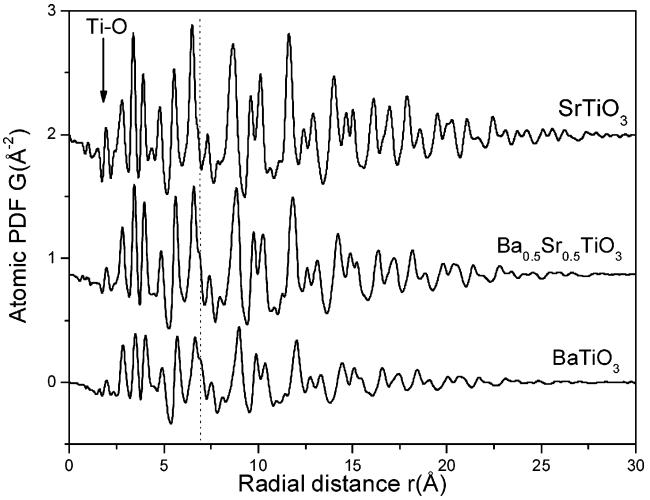


**Figure 3.** Experimental PDFs for nanocrystalline $Ba_xSr_{1-x}TiO_3$ extracted from the corresponding powder diffraction patterns using data extending to wave vectors as high as 28 $Å^{-1}$. The position of the first PDF peak, reflecting Ti−O first neighbor atomic pairs, is marked with an arrow. Note the intensity of the first PDF peak changes with the relative Sr/Ba content due to the different scattering power for X-rays of Ba and Sr. A broken line runs, as a guide to the eye, through the shoulder of the PDF peak centered at approximately 6.7 Å. The shoulder diminishes with Sr content.

This observation shows that the nanocrystalline $Ba_xSr_{1-x}TiO_3$ not only lacks the extended order of usual crystals but shows some structural distortions that further reduce their structural coherence. Such structural distortions are frequently observed with nanoparticles of sizes from 5−10 nm and are often ascribed to surface relaxation effects.[35] The distortions are more pronounced with nanocrystalline $BaTiO_3$ than with the samples containing Sr since its PDF decays to zero faster than those of the other two materials (see Figure 3). The first peak in the three experimental PDFs shown in Figure 3 is positioned at approximately 1.98(2) Å, which is close to the average Ti−O first neighbor distance observed in the corresponding crystalline bulk perovskites. The area under the peak yields 5.8(2) oxygen neighbors for each titanium atom, reflecting the presence of $Ti-O_6$ octahedral units in the nanomaterials. The peak is quite sharp and appears with almost the same shape and full-width at half-maximum (∼0.18 Å) in the PDFs for the three samples showing that they all are built of well-defined $Ti-O_6$ octahedra. Also, the three experimental PDFs exhibit a similar oscillatory behavior at longer interatomic distances, indicating that nanocrystalline $Ba_xSr_{1-x}TiO_3$ ($x = 1, 0.5, 0$) share common structural features, those of an extended network of $Ti-O_6$ octahedra. However, some fine but clearly noticeable differences in the experimental PDFs are also observed. For example, the peak at approximately 6.7 Å appears with a well-pronounced shoulder in the PDF for $BaTiO_3$. The same peak in the PDF for $SrTiO_3$ has no such pronounced shoulder. In general, the initial analysis of the experimental PDFs suggests that the atomic ordering in $Ba_xSr_{1-x}TiO_3$ nanopowders is likely to be of the same type but differ in some fine details for different concentrations of Ba and Sr. To reveal the fine features in the atomic ordering in nanocrystalline $Ba_xSr_{1-x}TiO_3$, we tested several structural models

(35) Gilbert, B.; Huang, F.; Zhang, H. Z.; Waychunas G. A.; Banfield, J. F. *Science* **2004**, *305*, 65.

**Table 1. Structure Data for Nanocrystalline $Ba_xSr_{1-x}TiO_3$ ($x = 1$, 0.5, 0) as Obtained by the Present Rietveld and PDF Refinements[a]**

| | $BaTiO_3$ | | $Ba_{0.5}Sr_{0.5}Ti\ O_3$ | | $SrTiO_3$ | |
|---|---|---|---|---|---|---|
| | Rietveld | PDF | Rietveld | PDF | Rietveld | PDF |
| *a*, Å | 4.016(6) | 4.021(5) | 3.985(4) | 3.979(6) | 3.930(3) | 3.927(5) |
| $U_{Ba/Sr}$ ($Å^2$) | 0.022(2) | 0.009(2) | 0.014(2) | 0.016(2) | 0.013(2) | 0.009(2) |
| $U_{Ti}$ ($Å^2$) | 0.016(2) | 0.015(2) | 0.013(2) | 0.006(2) | 0.008(2) | 0.010(2) |
| $U_O$ ($Å^2$) | −0.001(2) | 0.022(2) | 0.001(2) | 0.030(2) | 0.012(2) | 0.031(2) |
| Rw, % | 2.81 | 25 | 2.37 | 19 | 2.34 | 18 |

[a] The refinements are based on the cubic-type structure presented in Figure 1a. The goodness-of-fit (Rietveld, see eq 4) and reliability (PDF, see eq 5) factors $R_w$ are reported for each of the refinements.

analyzing the experimental diffraction data both in reciprocal and real space employing the Rietveld and PDF techniques, respectively.

## 4. Discussion

At first, we approached the experimental XRD patterns with the widely employed Rietveld technique. The Rietveld technique[36] is used for crystal structure determination and refinement from powder diffraction data. The method employs a least-squares procedure to compare experimental Bragg intensities with those calculated from a plausible structural model. The parameters of the model are then adjusted until the best fit to the experimental diffraction data is achieved. The progress of the fit is assessed by computing various goodness-of-fit factors with the most frequently used being[37]

$$R_w = \left\{ \frac{\sum w_i (y_i^{obs} - y_i^{calc})^2}{\sum w_i (y_i^{obs})^2} \right\}^{1/2} \quad (4)$$

where $y_i^{obs}$ and $y_i^{calc}$ are the observed and calculated data points and $w_i$ are weighting factors taking into account the statistical accuracy of the diffraction experiment. The Rietveld analyses were carried out with the help of the program FullProf.[38] The XRD patterns of nanocrystalline $SrTiO_3$ and $Ba_{0.5}Sr_{0.5}TiO_3$ were fit with a cubic structure of a perovskite type[39,11] that is found with the corresponding bulk crystals at room temperature. The XRD pattern of $BaTiO_3$ was approached with both the cubic and tetragonal structures (see Figures 1a and 1b) occurring with the corresponding bulk crystal. Results from the Rietveld refinements are presented in Figure 2 and the values of the refined structural parameters in Tables 1 and 2. As can be seen in Figure 2, the XRD pattern of $SrTiO_3$ and $Ba_{0.5}Sr_{0.5}TiO_3$ are very well reproduced by a model based on the cubic structure of a perovskite type shown in Figure 1a. The results show that even when in the nanocrystalline state, $SrTiO_3$ and $Ba_{0.5}Sr_{0.5}TiO_3$ adopt the structure type of the corresponding bulk crystals. The XRD pattern for nanocrystalline $BaTiO_3$ is almost equally well reproduced by the cubic and tetragonal perovskite-type structure as the data presented in Figure 2 shows. The values of the corresponding goodness-of-fit factors $R_w$, see Tables

(36) Rietveld, H. M. *J Appl. Crystallogr*. **1969**, *2*, 65.
(37) Young, R. A. In *The Rietveld Method*; Oxford University Press: New York, 1996.
(38) Rodríguez-Carvajal, J. *Physica B* **1993**, *192*, 55.
(39) Abramov, Y. A.; Tsirel'son, V. G.; Zavodnik, V. E.; Ivanov, S. A.; Brown, I. D. *Acta Crystallogr. B* **1983**, *39*, 942.

**Table 2. Structure Data for Nanocrystalline $BaTiO_3$ as Obtained by the Present Rietveld and PDF Refinements[a]**

| | Rietveld | PDF |
|---|---|---|
| *a*, Å | 3.987(6) | 3.997(6) |
| *c*, Å | 4.091(7) | 4.0851(7) |
| *z*(Ti) | 0.467(5) | 0.470(3) |
| *z*(O1) | −0.138(5) | −0.130(7) |
| *z*(O2) | 0.495(6) | 0.490(3) |
| $U_{Ba}$ (Å$^2$) | 0.027(2) | 0.010(2) |
| $U_{Ti}$ (Å$^2$) | 0.006(2) | 0.018(2) |
| $U_O$ (Å$^2$) | −0.020(2) | 0.021(2) |
| $R_w$, % | 2.47 | 21 |

[a] The refinements are based on the tetragonal-type structure presented in Figure 1b. The goodness-of-fit (Rietveld, see eq 4) and reliability (PDF, see eq 5) factors $R_w$ are reported for each of the refinements.

1 and 2, does not allow one to draw a definitive conclusion in favor of either of the two different structure models attempted either. Moreover, the Rietveld analysis of the XRD data for the nanocrystalline $BaTiO_3$ yielded negative values for the mean-square atomic displacements of oxygen atoms (also known as thermal factors; see Tables 1 and 2). Such unphysical results are often obtained with Rietveld analyses of powder diffraction patterns for materials with considerably reduced structural coherence. The problems stem from the inability of the Rietveld analysis to handle properly diffraction patterns showing both broad Bragg peaks and pronounced diffuse scattering. As we demonstrate below, the difficulties are greatly reduced when the diffraction data are analyzed in terms of the corresponding atomic PDFs. Similarly to the Rietveld technique, the PDF technique employs a least-squares procedure to compare experimental and model data (PDF) calculated from a plausible structural model. The structural parameters of the model (unit cell constants, atomic coordinates, and thermal factors) are adjusted until the best possible fit to the experimental data is achieved. The progress of the refinement is assessed by computing a reliability factor, $R_w$:

$$R_w = \left\{ \frac{\sum w_i (G_i^{exp.} - G_i^{calc.})^2}{\sum w_i (G_i^{exp.})^2} \right\}^{1/2} \quad (5)$$

where $G^{exp.}$ and $G^{calc.}$ are the experimental and calculated PDFs, respectively, and $w_i$ are weighting factors reflecting the statistical quality of the individual data points.

Results from the PDF analyses of the experimental data for $Ba_xSr_{1-x}TiO_3$ ($x = 1$, 0.5, 0) in terms of the cubic structure are presented in Figures 4 , 5, and 6. Structure data from literature sources[3,40−42] were used as initial values in the PDF refinements. The PDF refinements were done with the help of the program PDFFIT.[43] To mimic the presence of limited structural disorder in the nanocrystalline materials, we multiplied the model PDF data with a decaying exponent of the type $\exp(-\alpha r)$ as originally suggested by Ergun and later on implemented in a similar manner by Gilbert et al.[44] Typical values for $\alpha$ used were of the order of 0.1 Å$^{-1}$. The

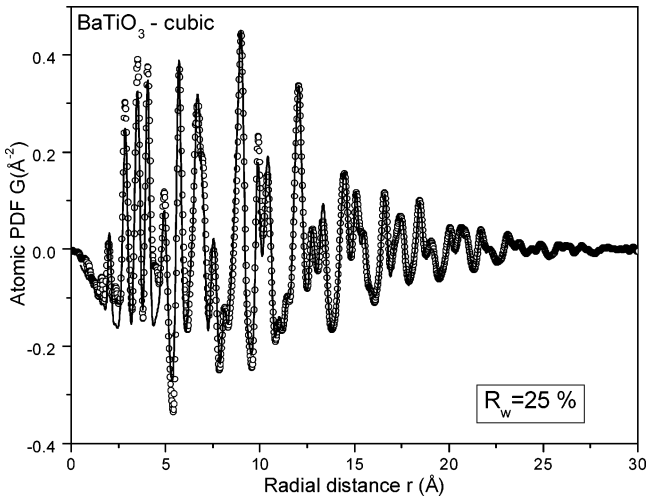


**Figure 4.** Experimental (symbols) and model (solid line) PDFs for $BaTiO_3$. The model PDF is based on the cubic-type structure shown in Figure 1a. The parameters of the model are given in Table 1. The reliability factor $R_w$ is reported in the lower part of the figure.

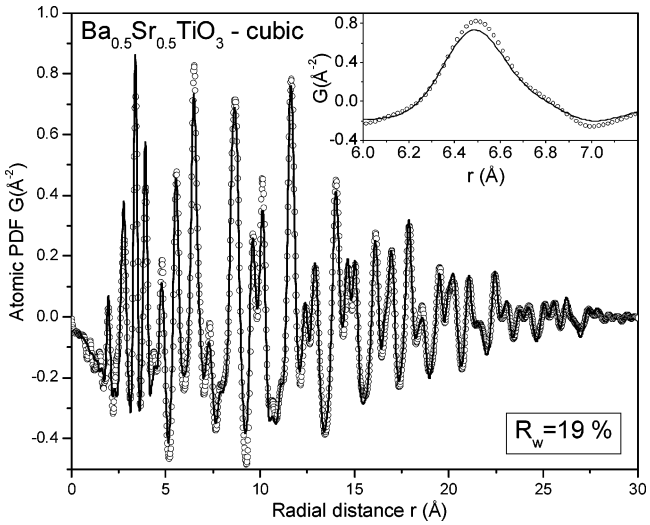


**Figure 5.** Experimental (symbols) and model (solid line) PDFs for $Ba_{0.5}Sr_{0.5}TiO_3$. The model PDF is based on a structure of the cubic type shown in Figure 1a. The parameters of the model are given in Table 1. The reliability factor $R_w$ is reported in the lower part of the figure. The peak at 6.7 Å is given an enlarged scale in the inset. Its shape is well-reproduced by a cubic-type model.

refined values of the structural parameters from the analysis are summarized in Table 1. In the case of $SrTiO_3$ and $Ba_{0.5}Sr_{0.5}TiO_3$ the PDF-based fit yielded structural parameters that are in good agreement with the present Rietveld results (see Table 1). The agreement documents well the fact that the atomic PDF provides a firm quantitative basis for structure determination. The reliability factors (defined by eq 5) also reported in Table 1 are as low (∼18%) as could be achieved with a PDF refinement.[45] These results support the findings of the Rietveld refinements that the atomic ordering in nanocrystalline $SrTiO_3$ and $Ba_{0.5}Sr_{0.5}TiO_3$ can be well-described in terms of the perovskite, cubic-type structure (space group $Pm\bar{3}m$) depicted in Figure 1a. Models based on the perovskite, tetragonal-type structure (space group *P*4*mm*) were also attempted with the PDF data for $SrTiO_3$ and $Ba_{0.5}Sr_{0.5}TiO_3$. These models, although having more internal degrees of freedom, did not give any significant

(40) Buttner, R. H.; Maslen, E. N. *Acta Crystallogr*. **1983**, *39*, 7764.
(41) Evans, H. T. *Acta Crystallogr*. **1967**, *1*, 1948.
(42) Hewat, A. W. *Ferroelectrics* **1974**, *6*, 215.
(43) Proffen, T.; Billinge, S. J. L. *J. Appl. Crystallogr*. **1999**, *32*, 572.
(44) Ergun, S.; Schehl, R. R. *Carbon* **1973**, *11*, 127. Gilbert, B.; Huang, F.; Zhang, H. Z.; Waychunas, G. A.; Banfield, J. F. *Science* **2004**, *305*, 65.

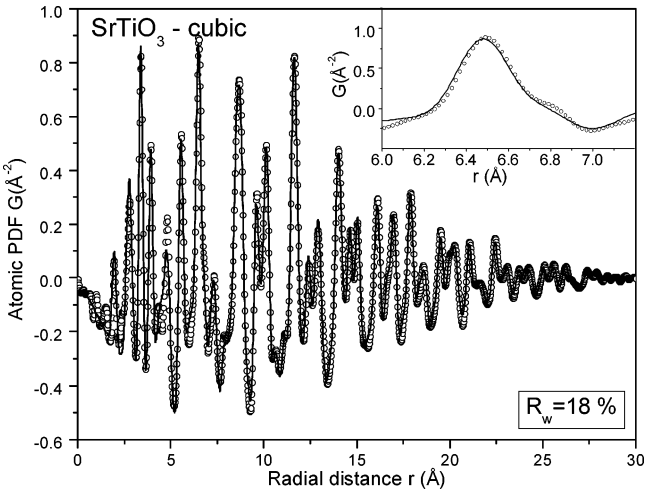


**Figure 6.** Experimental (symbols) and model (solid line) PDFs for $SrTiO_3$. The model PDF is based on a structure of the cubic type shown in Figure 1a. The parameters of the model are given in Table 1. The reliability factor $R_w$ is reported in the lower part of the figure. The peak at 6.7 Å is given an enlarged scale in the inset. Its shape is well-reproduced by a cubic-type model.

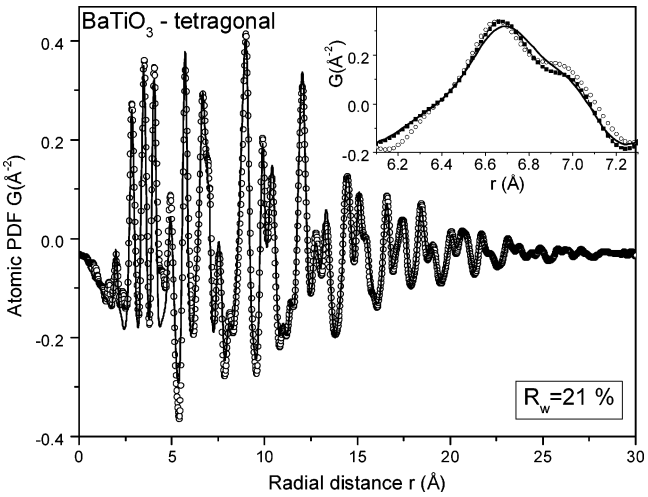


**Figure 7.** Experimental (symbols) and model (solid line) PDFs for $BaTiO_3$. The model PDF is based on the tetragonal-type structure shown in Figure 1b. The parameters of the model are given in Table 2. The reliability factor $R_w$ is reported in the lower part of the figure. A portion of the experimental data (open circles) is compared to model ones based on cubic-type (solid line) and tetragonal-type structures (solid symbols) in the inset on an enlarged scale. The experimental data are better reproduced by the tetragonal-type model.

improvement in the reliability factors nor in reproducing the important details in the experimental data. This observation reinforced our conclusion that nanocrystalline $SrTiO_3$ and $Ba_{0.5}Sr_{0.5}TiO_3$ studied by us possess a cubic-type structure at room temperature as their crystalline analogues do.

The atomic ordering in $BaTiO_3$, however, is not so well-described in terms of the perovskite, cubic-type structure as the relatively high value (~25%, see Table 1) of the corresponding reliability factor $R_w$ shows. That is why we attempted three more structural models based on the other three structural modifications: tetragonal (space group *P*4*mm*), orthorhombic (space group *Amm*2), and rhombohedral (space group *R*3*m*), occurring with bulk crystalline $BaTiO_3$. Results from PDF analyses of the experimental data in terms of these three structural models are presented in Figures 7, 8, and 9, respectively. As the results in Figures 8 and 9 show, the orthorhombic- and rhombohedral-type models (see Figures 1c and 1d) may be unambiguously ruled out because they feature substantially distorted $Ti-O_6$ octahedral units, i.e., a broad distribution of first neighbor Ti−O distances (2 Ti−O distances at 1.86 Å, two Ti−O distances of 2.0 Å, and two Ti−O distances of 2.16 Å with the orthorhombic model; three Ti−O distances of 1.87 Å and three Ti−O distances of 2.13 Å with the rhombohedral model) resulting in a split first PDF peak, a feature the experimental data do not show. On the other hand, the model based on the tetragonal-type structure considerably improves the reliability factor (compare the PDF-based $R_w$ values reported in Tables 1 and 2 calculated over the whole range of PDF data from 1 to 28 Å) and better describes the fine features in the experimental PDF data appearing at low-*r* values, in particular, the intensity distribution of the two subcomponents of the split PDF peak at 10 Å and the position and intensity of the shoulder of the peak at 6.9 Å (see the inset in Figure 7). The shoulder reflects mostly correlations between oxygen atoms from neighboring $Ti-O_6$ octahedra and its pronounced presence in the PDF for $BaTiO_3$ and

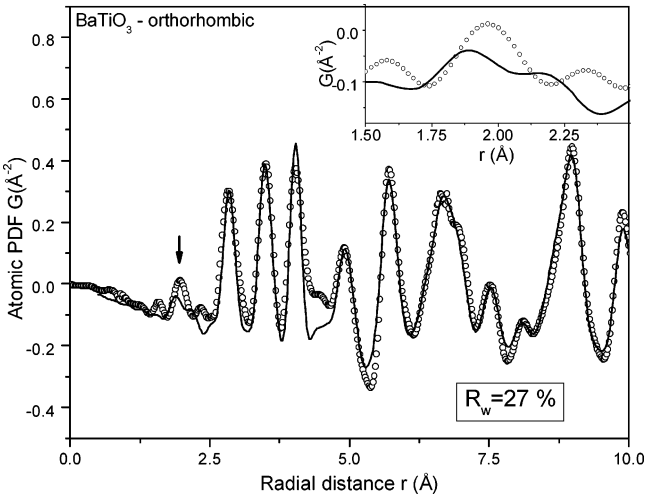


**Figure 8.** Experimental (symbols) and model (solid line) PDFs for $BaTiO_3$. The model PDF is based on the orthorhombic-type structure shown in Figure 1c. The reliability factor $R_w$ is reported in the lower part of the figure. An arrow marks the position of the first PDF peak where the model and experimental data show a strong disagreement. The same peak is given in the inset on an enlarged scale.

(45) Here it may be noted that the agreement factors achieved with the PDF refinements appear somewhat higher when compared to those resulted from the Rietveld refinement of diffraction data in reciprocal space (see Tables 1 and 2). This reflects the fact that an atomic PDF differs from the corresponding XRD pattern and is a quantity much more sensitive to the local atomic ordering in materials. Furthermore, the PDF $G(r)$ is very sensitive to the effects of imperfect data correction and systematic errors. As a result, $R_w$'s close to 20% are common for PDF refinements even of well-crystallized materials.[21,23,31] The inherently higher absolute value of the reliability factors resulting from PDF-based refinements does not affect their functional purpose as a residuals quantity that must be minimized to find the best fit and as a quantity allowing differentiation between competing structural models. It may also be noted that when the atomic pair correlation function, $g(r)$, defined as $g(r) = \rho(r)/\rho_0$, is used to guide a refinement of a structural model, the resulting reliability factors $R_w$ are significantly lower than those reported from a refinement based on the corresponding PDF $G(r)$, and very close to the values of the goodness-of-fit indicators reported from Rietveld analyses. We, however, prefer to work with the PDF $G(r)$ and not $g(r)$ since the former scales with the radial distance $r$ (see the multiplicative factor in the definition of $G(r)$; eq 1) and is thus more sensitive to the longer range atomic correlations.

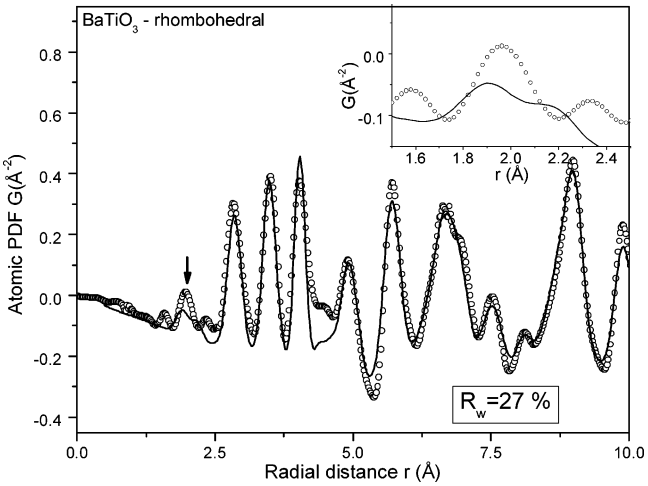


**Figure 9.** Experimental (symbols) and model (solid line) PDFs for $BaTiO_3$. The model PDF is based on the rhombohedral-type structure shown in Figure 1d. The reliability factor $R_w$ is reported in the lower part of the figure. An arrow marks the position of the first PDF peak where the model and experimental data show a strong disagreement. The same peak is given in the inset on an enlarged scale.

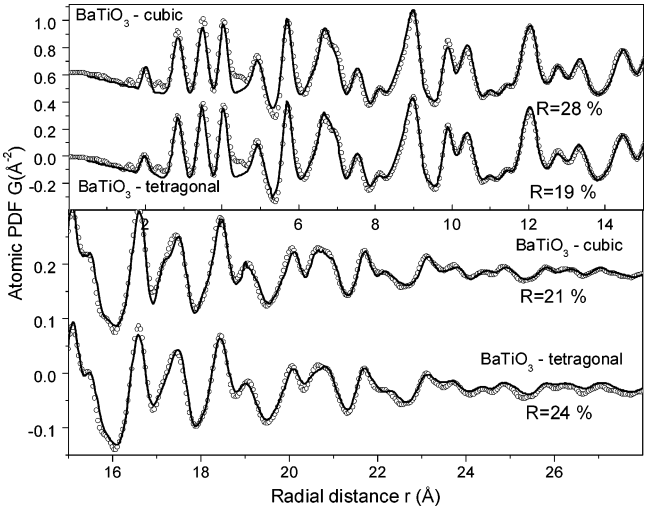


**Figure 10.** Low $r$ (0−15 Å; upper panel) and higher $r$ part (15−28 Å; lower panel) of the experimental (symbols) and model (solid line) PDFs for $BaTiO_3$. The model PDFs are based on the cubic- and tetragonal-type structures shown in Figure 1a and 1b, respectively. The corresponding structural parameters are summarized in Table 1 and Table 2, respectively. The reported in the figure reliability factors $R_w$ are calculated over the corresponding range of distances.

almost disappearance in the PDFs for $SrTiO_3$ and $Ba_{05}Sr_{0.5}$-$TiO_3$ (see Figure 3) indicates that those octahedral units are somewhat distorted/rotated in the former material and almost perfectly lined up in the materials containing Sr. The results suggest that the atomic ordering in nanocrystalline $BaTiO_3$ studied by us is likely to exhibit slight distortions similar to those occurring in bulk tetragonal $BaTiO_3$ crystal.

The tetragonal structure too features somewhat distorted $Ti-O_6$ octahedra (one Ti−O distance of approximately 1.9 Å, four Ti−O distances of 2.0 Å, and one Ti−O distance of 2.15 Å). The first peak in the PDF for nanocrystalline $BaTiO_3$, however, is very well reproduced by the tetragonal-based model, indicating that a model featuring slightly distorted $Ti-O_6$ octahedra is compatible with the experimental diffraction data. Interestingly, the tetragonal-based model is superior over the cubic one mostly at low-$r$ distances (0−15 Å) as the data in Figure 10 a show. It also agrees reasonably well with the PDF data at higher $r$ distances and yields a better overall reliability factor $R_w$ (see Figure 7). A closer look at the behavior of the model data at higher $r$ distances, however, shows (see Figure 10b) that the cubic-based model somewhat outperforms the tetragonal-based one as the corresponding reliability factors $R_w$ (this time calculated over a range of real space distances from 15 to 28 Å) shows. For longer range distances the tetragonal-structure-based model does not reproduce the intensities of the experimental PDF peaks as good as the cubic-type models do and, furthermore, seems to produce a PDF that is not perfectly lined up with the experimental data for distances longer than 24 Å. The fact that the tetragonal-type model is superior over the cubic-type one mostly at distances shorter than 10−15 Å shows that the fine tetragonal distortions in nanocrystalline $BaTiO_3$ are very likely to be local in nature (up to 10−15 Å) and coexist with a cubic-type arrangement at longer range interatomic distances. The coexistence of a lower symmetry local and a higher symmetry average atomic arrangements is not an unusual picture and has even been observed with perfectly crystalline materials such as In−Ga−As semiconductors for example. These are single-phase materials possessing a long-range cubic structure and substantially distorted local atomic ordering.[29] Nanocrystalline $ZrO_2$ has also shown a distorted local and cubic-type, longer range atomic structure.[33] Furthermore, recent NMR studies[46] have suggested that even bulk cubic $BaTiO_3$ crystal may be viewed as an assembly of a large number of small and randomly oriented "tetragonal" nanosize domains with dynamically elongated unit cells which transform into a phase with macroscopic tetragonal structure only when cooled below 393 K. With nanocrystalline $BaTiO_3$ such a transformation of the local tetragonal-type distortions into a macroscopic tetragonal-type structure that is thermodynamically stable at room temperature may not occur because of the very limited structural coherence length (∼2 nm) in the material.

In summary, the results of our structural studies show that nanocrystalline $SrTiO_3$ and $Ba_{0.5}Sr_{0.5}TiO_3$ possess a structure of a perovskite type exhibiting almost perfect $Ti-O_6$ units arranged in a long-range pattern with cubic symmetry. The atomic arrangement in nanocrystalline $BaTiO_3$ is also of a perovskite type but exhibits slight tetragonal distortions that show up at short-range interatomic distances only.

This new structural information helps one understand the dielectric properties of $Ba_xSr_{1-x}TiO_3$ ($x = 1$, 0.5, 0) nanoceramics as follows: The longer range cubic (centrosymmetric structures) of $SrTiO_3$ and $Ba_{0.5}Sr_{0.5}TiO_3$ are incompatible with the appearance of ferroelectricity and the materials do not show spontaneous polarization as experimentally observed.[12−16] The situation with $BaTiO_3$ is more complex. The material shows local tetragonal distortions but they seem to be confined to distances as short as 10−15 Å only. As the theoretical estimates of Lines and Glass suggest,[47] the correlation length between polar units in

(46) Zalar, B.; Lebar, A.; Selinger, J.; Blinc, R. *Phys. Rev. B.* **2005**, *71*, 064107.
(47) Lines, M. E.; Glass, A. M. In *Principles and Applications of Ferroelectrics and Related Materials*; Clarendon: Oxford, 1977.

ferroelectric materials are of the order of at least 10 and 2 nm in directions parallel and perpendicular to the polarization vector, respectively. With nanocrystalline $BaTiO_3$ the polar units (slightly distorted/rotated $Ti-O_6$ octahedra) are correlated over distances of about 1.5 nm only and may not become a driving force strong enough to transform the longer range structure into an asymmetric (tetragonal) one even at room temperature. As a result, the material does not show macroscopic spontaneous polarization as observed in practice.[12−16]

## 5. Conclusions

The atomic arrangement in nanocrystalline $Ba_xSr_{1-x}TiO_3$ ($x = 1, 0.5, 0$) has been studied by synchrotron radiation scattering experiments and Rietveld and atomic PDF techniques. The materials have been found to possess an atomic arrangement well-defined over 2−2.5 nm distances and resembling the one occurring in the crystalline perovskites. Although the structural coherence length in the nanostructured materials is greatly reduced, their structure still may be described in terms of a repetitive unit cell containing only a few atoms as the data summarized in Tables 1 and 2 show. $SrTiO_3$ and $Ba_{0.5}Sr_{0.5}TiO_3$ possess an atomic arrangement that is cubic type at both short and longer range interatomic distances. The local symmetry with nanocrystalline $BaTiO_3$ is tetragonal but the slight tetragonal distortions seem to average out and the structure of the material is better described in terms of a cubic-like ordering at longer range distances. That is presumably the reason nanocrystalline $BaTiO_3$, similarly to $SrTiO_3$ and $Ba_{0.5}Sr_{0.5}TiO_3$, does not show spontaneous polarization at room temperature.

This study is another demonstration of the ability of the PDF technique to yield three-dimensional structural information for materials of limited structural coherence, including nanocrystalline materials. The technique succeeds because it relies on total scattering data obtained from the material and, as a result, is sensitive to its essential structural features regardless of crystalline periodicity and size.

**Acknowledgment.** Thanks are due to M. Beno from APS, Argonne National Laboratory, for the help with the synchrotron experiments. The work was supported by NSF through grant DMR 0304391(NIRT). The Advanced Photon Source is supported by DOE under Contract W-31-109-Eng-38.

CM052145G